Physical properties of fixed-charge layer double hydroxides

D. R. Hines and S. A. Solin
NEC Research Institute, Princeton, New Jersey 08540

Umberto Costantino and Morena Nocchetti
Dipartimento di Chimica, Università di Perugia, Via Elce di Sotto, 8, 06123 Perugia, Italy

(Received 29 July 1999)

The physical properties of a series of layer double hydroxides (LDH) of the form $[(CO_3)_{0.195(1-x)}Cl_{0.39x}(H_2O)_y]:[Zn_{0.61}Al_{0.39}(OH)_2]$, $0 \leqslant x \leqslant 1$, $0 \leqslant y \leqslant (0.4+0.2x)$ have been studied. The hydration dynamics of these materials indicate that the guest layer water molecules form a hydration ring which defines the height of the solvated, nested Cl anion. The water molecules can tilt around their C_{2v} axis such that the height of the solvated Cl ion is a function of the number of molecules forming the hydration ring. The composition dependence of the basal spacing, determined from x-ray-diffraction powder patterns measured as a function of humidity and temperature for these materials, is a function of both the Cl concentration (x) and the number of guest layer water molecules (y). Distinct basal spacing curves are observed for fully hydrated, partially hydrated, and dehydrated materials. At $x=1$ the Cl end-member material exhibits a change in stacking sequence from a $3R$ polytype to a $2H$ polytype upon dehydration. The dehydrated form of this material also exhibits a $(\sqrt{3}\times\sqrt{3})R30°$ superlattice ordering of the Cl ions. Due to the nesting of the Cl ion and the active nature of the water molecules, the basal spacing vs x curve for the dehydrated materials is the only curve that can be fit by the discrete finite layer rigidity model. The interlayer rigidity parameter for LDH materials has been determined to be $p=4.84\pm0.06$ indicating that these materials are stiffer than class-II layered solids but not as stiff as class-III layered solids.

I. INTRODUCTION

Layer double hydroxides (LDH's) constitute a unique class of layered solids comprised of positively charged, brucitelike layers separated by charge balancing anions. Due to the mobility of the anions, these materials have important applications in fields such as catalysis,[1] chemical additives,[2] *in situ* remediation of contaminated soil,[3] photophysical and photochemical devices,[4] and battery technology.[5] The anionic mobility of LDH materials depends on both the physical properties and the hydration dynamics of these compounds. Two physical properties of fundamental interest in the study of intercalated layered solids are (i) the layer rigidity[6] which relates the basal spacing expansion to the change in anionic composition and (ii) the hydration dynamics.[7] Thus it is desirable to study both the layer rigidity and hydration dynamics of LDH materials. Until recently, for intercalated layered solids, these two physical properties have been treated separately such that the relative concentration of water in the guest layer has been viewed as having a negligible effect on the basal spacing (provided that the material does not undergo a water layer hydration state phase transition[8]). We will show in this paper that this is not the case for certain LDH materials.

Layer double hydroxides are materials of the general formula $[A^{n-}_{(z/n)(1-x)}B^{m-}_{(z/m)(x)}S_y]^{-z}:[M(\mathrm{II})_{1-z}M(\mathrm{III})_z(\mathrm{OH})_x]^{+z}$ where $M(\mathrm{II})$ is a divalent cation (Mg, Fe, Ni, Zn, ...), $M(\mathrm{III})$ is a trivalent cation (Al, Fe, Cr, ...), A^{n-} (B^{m-}) is a smaller (larger) charge compensating anion (CO_3^{2-}, SO_4^{2-}, NO_3^-, Cl^-, Br^-, ...) and S is a co-intercalated solvent molecule (usually H_2O). The second bracketed term in the chemical formula represents the host layer which is comprised of divalent cations each octahedrally coordinated to six hydroxyl groups. For each hydroxyl group, the oxygen atom is shared by three cations and the hydrogen atom is oriented toward the adjacent host layer. The host layer acquires a net positive charge due to isomorphic substitution of $M(\mathrm{II})$ divalent cations by $M(\mathrm{III})$ trivalent cations. The space between host layers is referred to as the gallery and usually contains a guest layer which is represented by the first bracketed term in the chemical formula. Anionic species are intercalated into the gallery in order to maintain overall electroneutrality. In general, the anions do not fill all the available sites within the guest layer; thus additional solvent molecules tend to co-intercalate. Two main subgroups of LDH materials can be delineated where the guest layer composition can be varied either independent of the host layer *via* ion-exchange (i.e., fixed-host layer materials where z is a fixed value and x is varied) or as a result of cation substitutions within the host layer (i.e., variable-host layer materials where z is varied and x is either fixed or variable). Previous layer rigidity studies of LDH compounds have been conducted using variable-host layer materials of the form $[(CO_3)_{z/2}(H_2O)_y]:[Ni_{1-x}Al_z(OH)_2]$, $0 \leqslant z \leqslant 0.4$, $0 \leqslant y \leqslant 1.2$ [hereafter referred to as $(CO_3)(\mathrm{NiAl}):\mathrm{LDH}$].[9] For these materials, a concomitant change within both the host (intra-) and guest (inter-) layers results in transverse distortions of the host layer (e.g., displacements perpendicular to the plane of the layers). The standard discrete finite layer rigidity (FLR) model,[10] which successfully accounts for the composition-dependence of the basal spacing of a wide variety of intercalated layered solids, incorporates only an interlayer rigidity parameter. Thus it does not properly account for the basal spacing response as a function of guest layer anionic concentration for this variable-host layer LDH.[9] The interlayer rigidity parameter relates the change in anionic concentration within the guest layer to the change in basal spacing and hence does not explicitly account for cation sub-

stitution within the host layer. Therefore an intralayer rigidity parameter was introduced in order to account for the cation substitution within the host layer.[9] This was accomplished by developing an extended version of the discrete FLR model which contains both an interlayer and an intralayer rigidity parameter.[9] A fit using this model to the basal spacing as a function of CO_3 concentration for a series of (CO_3)(NiAl):LDH materials resulted in an intralayer rigidity parameter of $q=2.44$ and an interlayer rigidity parameter of $p\sim 5$.[9] The approximate nature of the interlayer rigidity parameter is due to the multiparameter aspect of the extended FLR model and the presence of water molecules in the guest layer. These water molecules solvate the CO_3 ions thus producing a composite ion that is essentially unchanged in height (the oxygen atom defines the height of both the water molecule and the carbonate ion) but larger in lateral extent as compared to the bare CO_3 ion. The larger lateral size of the composite ion increases the local basal spacing over a larger area resulting in a larger average basal spacing for the material. This larger average basal spacing causes the host layer to appear to be too stiff. In order to account for this effect, the interlayer rigidity parameter must be rescaled thus resulting in only an approximate value of p.

As compared to the variable-host layer LDH materials described above, it will be shown in this paper that a study of fixed-host layer LDH materials alleviates the need for introducing an intralayer rigidity parameter. The materials utilized in this study are the dehydrated form of a series of compounds having a chemical formula

$$[(CO_3)_{0.195(1-x)}Cl_{0.39x}(H_2O)_y]:[Zn_{0.61}Al_{0.39}(OH)_2],$$

$$0\leqslant x\leqslant 1,\ \ 0\leqslant y\leqslant (0.4+0.2x)$$

[hereafter referred to as (CO_3/Cl)(ZnAl):LDH].[11] Thus the standard discrete FLR model from which the interlayer rigidity parameter is determined to be $p=4.84\pm 0.06$ is sufficient to model the basal spacing response as a function of guest layer anion concentration. It is observed in these materials, however, that the basal spacing decreases as the concentration of the larger anion is increased. This retrograde response is due to a nesting of the larger Cl ion into the trigonal pockets of the host layer. This study shows that the layer rigidity of LDH materials has been successfully modeled using the standard discrete FLR model. The layer rigidity of these LDH materials will be compared directly with the layer rigidity of other layered solids such as graphite,[12] layer dichalcogenides,[13] and clays[14] which have also been successfully modeled using the standard discrete FLR model as noted above.

In addition to the layer rigidity of the dehydrated forms of these fixed-host layer LDH materials, the hydration dynamics exhibit a rich behavior. Previously the hydration dynamics of the end-member materials ($x=0$ and 1) have been studied.[11] For the CO_3 end-member material, the basal spacing is essentially independent of the water content of the guest layer. However, for the Cl end-member material, the basal spacing exhibits three distinctly different values depending on the amount of water present in the guest layer. The activity of the guest layer water molecules, in the presence of Cl ions, has been attributed to the interplay between a nesting of the Cl ions into the trigonal pockets of the host layer and a rotation of the water molecules around their C_{2v} axes as they solvate the ions.

In this paper, we will focus on the physical properties of fixed-host layer LDH materials as they are affected by changes in the relative concentration of guest layer anions (a change in x) and the number of water molecules in the guest layer (i.e., hydration dynamics—a change in y). This study will combine and expand the preliminary studies that have been previously reported for both the layer rigidity of the dehydrated materials[15] and the hydration dynamics of the end-member ($x=0$ and $x=1$) materials.[11] Interesting results along with the preliminary results will be incorporated into a fully detailed analysis of the (CO_3/Cl)(ZnAl):LDH materials having an arbitrary anionic concentration (i.e., any x value) and an arbitrary number of water molecules in the guest layer (i.e., any y value). It will be shown that the behavior of the water molecules as seen in the Cl end-member material is also manifest in the hydrated (CO_3/Cl)(ZnAl):LDH materials as the relative concentration of CO_3 to Cl ions reaches $x=0.5$. In addition to changes in the basal spacing, these LDH materials undergo a change in stacking sequence during dehydration. For example, the Cl end-member material, in its hydrated form, exhibits a $3R$ stacking sequence[16] with 10% faulting. Once dehydrated, the material converts to a $2H$ stacking sequence.[16] There is also evidence for a superlattice ordering of the Cl anions in the dehydrated materials. Extra x-ray-diffraction reflections appear which have been associated with a $(\sqrt{3}\times\sqrt{3})R30°$ structure.

II. EXPERIMENT

All LDH materials utilized in this study were synthesized from RP-ACS grade reagent. The (CO_3)(ZnAl):LDH carbonate end-member material was obtained using a procedure[17] based on the *in situ* formation of ammonium carbonate from urea. Materials with increasing Cl ion concentration ($x>0.0$) were obtained by an HCl titration method.[18] An additional set of materials were obtained from the resulting (Cl)(ZnAl):LDH, end-member material ($x=1.0$) using the ion-exchange, isotherm method.[18] Chemical analysis was performed using several different techniques depending on the chemical species of interest. These included ethylenediamine tetra-acetic acid titrations[19] for aluminum and zinc, carbon microanalysis for the carbonate content, and ion chromatography for the chloride content. Hydration water was calculated from the weight loss of the samples at 150 °C using a thermoanalyzer.

Thermogravimetric analysis (TGA) was performed using a Perkin-Elmer TGA7 instrument. In an N_2 purge, the weight of the sample was recorded as a function of time until equilibrium was reached. The sample was determined to be at equilibrium once the weight reached a constant value. The weight of the sample was then recorded as a function of temperature.

X-ray diffraction (XRD) powder patterns were measured using a rotating anode x-ray generator configured to produce a horizontal line source of Cu radiation. A bent crystal graphite monochromator was aligned with the x-ray generator to allow only Cu$K\alpha$ radiation to reach the sample. The

sample was mounted on a Huber four-circle diffractometer aligned to the Cu$K\alpha$ x-ray beam and configured to measure diffraction in the vertical plane. An Li drifted, NaI scintillation detector was mounted on the 2θ circle. The (003) and (006) Bragg reflections measured in the powder pattern were used in a q-plot[20] to determine the basal spacing.

For all samples in air at room temperature, a full XRD pattern was acquired. Subsequently an N_2 purge was established around the sample. As soon as the purge was started at room temperature, both the (003) and (006) reflections were repeatedly measured in order to monitor the basal spacing dynamics. During the first several hours these reflections were measured continuously and there after at 20 min intervals. A sample remained at room temperature in the N_2 purge until its weight reached equilibrium as determined by TGA measurements described above. Again, for all samples, a full XRD pattern was measured at this equilibrium condition. Initial hydration studies were performed on both the Cl and CO_3 end-member samples where, with the N_2 purge uninterrupted, the temperature was increased at a rate of 0.01 °/min and at certain temperatures, held fixed so that a full XRD pattern could be measured. During temperature ramps, the (003) and (006) reflections were again measured every 20 min. A similar procedure was utilized for all of the other (non-end-member) samples.

III. RESULTS AND DISCUSSION

A. Ion exchange

1. Forward carbonate-chloride ion exchange via acid-base titration

The synthesis procedure described above, accomplished by hydrolysis of urea, leads to a (CO_3)(ZnAl):LDH material with good crystallinity and a narrow distribution of particle size in the 5–15 μm range as determined from x-ray-diffraction powder patterns, particle size distribution measurements, scanning electron microscopy, and (SEM) micrographs. The composition of the as-grown, CO_3 end-member starting material was found to be $[(CO_3)_{0.195}(H_2O)_{0.4}]$:$[Zn_{0.61}Al_{0.39}(OH)_2]$ with an anion exchange capacity of 3.78 m equiv./g.

It is well known[21] that the CO_3 anions are strongly held in the interlayer region and that it is very difficult to replace them with other anions using simple ion-exchange processes. Alternative methods have been proposed[22] based on the protonation of the guest layer carbonate into carbon dioxide coupled with the insertion of another charge balancing anion. Samples of composition

$$[(CO_3)_{0.195(1-x)}Cl_{0.39x}(H_2O)_y]:[Zn_{0.61}Al_{0.39}(OH)_2],$$

with $0 \leqslant x \leqslant 1$ and $0 \leqslant y \leqslant (0.4+0.2x)$ have thus been obtained by such methods. Figure 1 shows the HCl titration curve (dotted line) and the associated uptake curve (solid line). For clarity, the percent of exchange [that is $x \cdot 100$, x = (m equiv. Cl^-)/(m equiv. $Cl^- +$ m equiv. CO_3^{2-}) in the solid] is reported on the top of the plot. The shape of the titration curve, and hence the uptake curve, is indicative of the ion-exchange mechanics[23–25] where the replacement of CO_3 ions with Cl ions proceeds in three steps. In the first step, $0 \leqslant x < 0.4$, the incoming Cl ions are solubilized in the

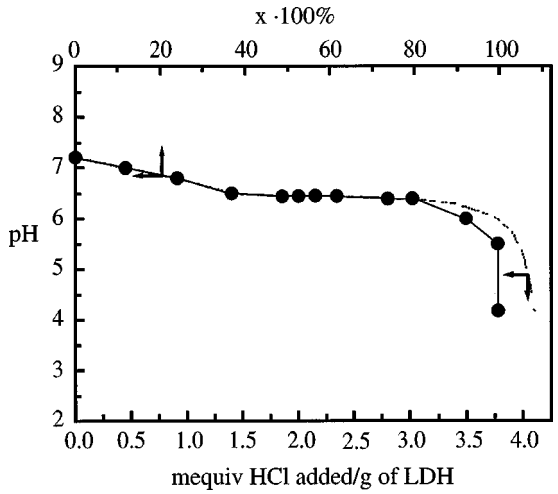

FIG. 1. The batch titration curve for (CO_3)(ZnAl):LDH with 0.1 mol/dm^3 HCl solution in the presence of NaCl as the added salt. Data points (solid curve) refer to the Cl ion uptake (top axis) and the dashed curve refers to the forward titration (bottom axis).

(CO_3)(ZnAl):LDH structure and a gradual decrease of pH of solution is observed. As this initial phase becomes saturated with Cl ions, the second step, $0.4 \leqslant x \leqslant 0.8$, takes place, at constant composition of solution, with the formation of the (Cl)(ZnAl):LDH phase. When the phase transition is complete, a single phase system is present and the pH changes with further HCl addition. The third step, $x > 0.8$, therefore corresponds to the solubilization of the CO_3 ions into the (Cl)(ZnAl):LDH phase.

XRD powder patterns have been measured for a suite of samples prepared by the acid-base titration method. The (006) reflections for these samples are shown in Fig. 2. The reflections associated with the end-member materials (open circles for $x = 1.0$ and open squares for $x = 0.0$) are well formed and symmetric which is an indication of single phase materials. However, the (006) reflections for samples having intermediate values of x exhibit multiple peaks. Each peak is associated with a distinct basal spacing. Since, for these fully hydrated materials, the basal spacing is larger for the Cl end-member material and smaller for the CO_3 end-member material, the distinct peaks for these intermediate x values can

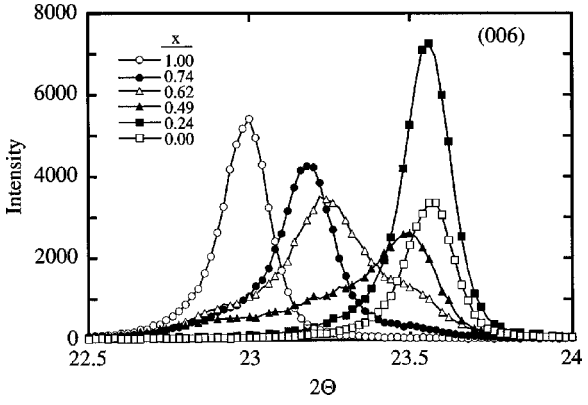

FIG. 2. The (006) reflection from XRD powder patterns as a function of Cl ion concentration (x) for a series of (CO_3/Cl)(ZnAl):LDH's which were ion exchanged using the titration method with (CO_3)(ZnAl):LDH as the starting material.

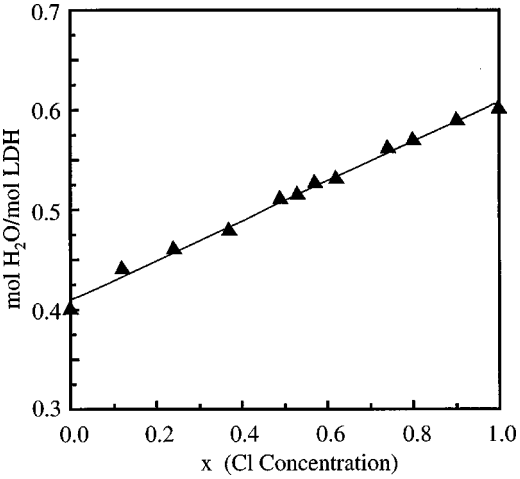

FIG. 3. The water content of $(CO_3/Cl)(ZnAl)$:LDH as a function of the Cl ion concentration (x).

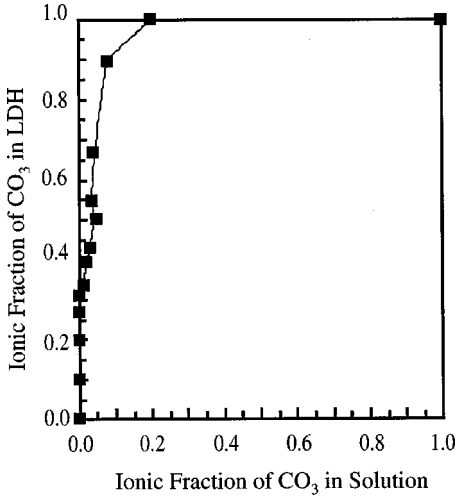

FIG. 4. The CO_3/Cl ion-exchange isotherm at an ionic concentration of 0.1 equiv./dm^3 at a temperature of $25° \pm 1°$.

be associated with both Cl rich (lower angle peaks) and CO_3 rich (higher angle peaks) regions within a given sample.

Even though the guest layer anions tend to phase separate, for intermediate values of x, the amount of hydration water is a linear function of the guest layer ionic concentration as seen in Fig. 3 and can be expressed as $y=0.4+0.2x$. In a fully hydrated material, the water molecules appear to fill all the available guest layer sites which are not occupied by a charge compensating anion. Because of the CO_3 ion is comprised of three oxygen atoms, it occupies three guest layer sites; therefore one water molecule is added to the guest layer for every CO_3 ion which is replaced by two Cl ions.

2. Reverse chloride-carbonate ion exchange via ion-exchange isotherm

Because of the phase separation which occurs for intermediate values of x in samples where the acid-base titration method of ion exchange was utilized, it is desirable to establish an alternative method of ion exchange. Therefore the ion-exchange isotherm method was used to prepare $(CO_3/Cl)(ZnAl)$:LDH materials from the Cl end-member material. Figure 4 shows the CO_3/Cl ion-exchange isotherm obtained at 25 °C and an ionic fraction of 0.1 equiv./dm^3. As expected, the isotherm is strongly shifted to the left. The (Cl)(ZnAl):LDH is completely converted to (CO_3)(ZnAl):LDH by the time the CO_3 ionic fraction in the solution reaches 27%. The preferential intercalation of the CO_3 ion into the guest layer results in a selectivity constant,[26] that is the quotient of the concentration ratios of the two counter ions in LDH and in solution, of about 20 at $x=0.5$. The XRD powder patterns of the $(CO_3/Cl)(ZnAl)$:LDH materials prepared using the ion-exchange isotherm method have been measured. The (006) reflections are illustrated in Fig. 5. These reflections are to be compared to those in Fig. 2 for samples prepared from the titration method. The reflections associated with the end-member materials (open circles for $x=1.0$ and open squares for $x=0.0$) in these two figures are from the same samples. As seen in Fig. 5, the (006) reflections for samples having intermediate values of x do not exhibit multiple peaks for the samples obtained from the ion-exchange isotherm method. This is in contrast to the multiple peaks seen in Fig. 2 for materials prepared from the titration method. Therefore materials prepared from the ion-exchange isotherm method are of more uniform composition and thus more single phase than materials prepared from the acid-base titration method. Hereafter, we consider only samples which have been prepared using the ion-exchange isotherm method.

B. Stacking sequence

X-ray-diffraction powder patterns for the Cl end-member material, (Cl)(ZnAl):LDH ($x=1$), are shown in Fig. 6 as a function of temperature for samples in an N_2 purge. Several features are evident in these patterns at temperatures below 170 °C. First, the prominent (00L) reflections seen below $2\theta=30°$ are indicative of layered solids. These reflections shift with temperature, indicating a change in the basal spacing of the material. At certain temperatures the (006) reflection splits into two reflections indicating the presence of two coexisting phases within the sample at that temperature. The basal spacing dynamics as determined from these (00L) reflections will be discussed below in conjunction with TGA

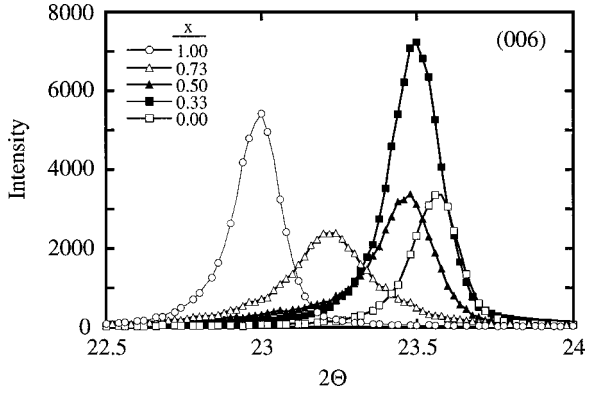

FIG. 5. The (006) reflection from XRD powder patterns as a function of Cl ion concentration (x) for a series of $(CO_3/Cl)(ZnAl)$:LDH's which were ion exchanged using the ion-exchange isotherm method with (Cl)(ZnAl):LDH as the starting material.

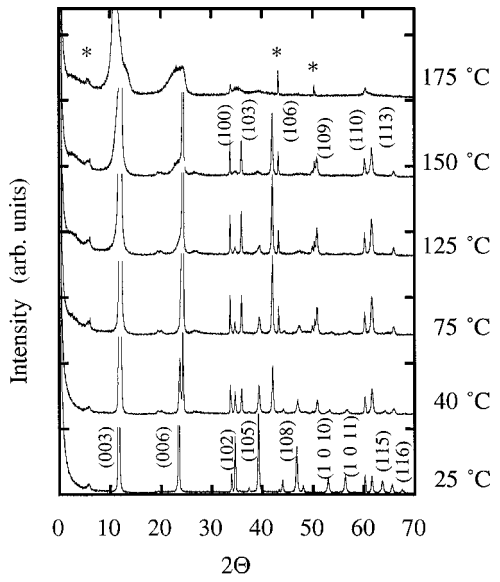

FIG. 6. Cu$K\alpha$ x-ray powder-diffraction patterns of (Cl)(ZnAl):LDH as a function of sample temperature in an N_2 purge. The patterns have been vertically displaced and the (003) and (006) reflections truncated for clarity. The * indicates reflections associated with the sample holder.

data in order to describe the hydration dynamics of the (CO_3/Cl)(ZnAl):LDH materials. Second, the narrow width of the (100) and (110) in-plane reflections indicate well formed crystallites as further evidenced by the SEM micrograph shown in Fig. 7 which reveals platelets as large as 10 μm in diameter. The Bragg angle and relative intensity of these two reflections do not change as the temperature of the sample is increased up to 150 °C indicating that the host layer is unchanged. Third, excluding the (00L), (100), and (110) reflections, the relative intensity of most of the remaining reflections changes as a function of temperature where some reflections appear as other reflections disappear. In fact, the change is so dramatic that one might be tempted to view the XRD patterns at 25 and 125 °C as having been produced by different materials. Actually, as will be mentioned below, this misleading view permeates the earliest literature[27,28] dealing with the nomenclature of LDH materials.

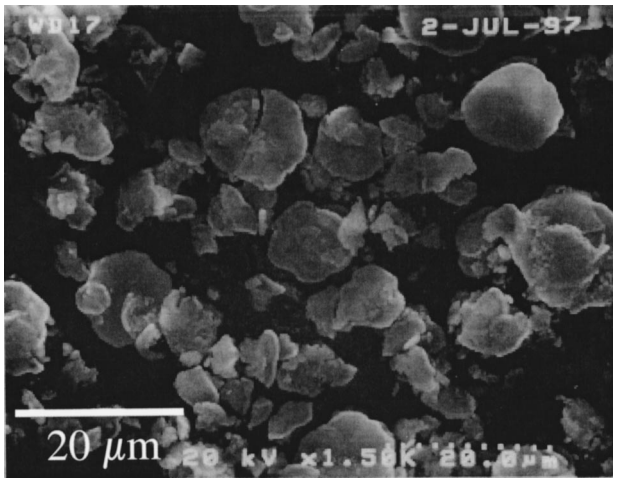

FIG. 7. A SEM micrograph of (Cl)(ZnAl):LDH.

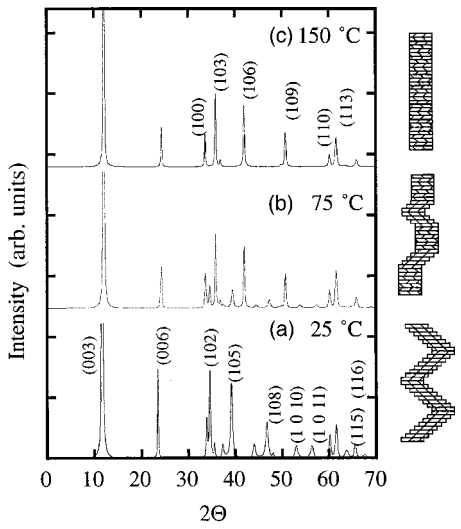

FIG. 8. Simulation Cu$K\alpha$ x-ray powder-diffraction patterns generated using DIFFaX (see text). Each pattern was generated using unit cell parameters $a=3.073$ Å and (a) $c=22.713$ Å and an $ABCABC\cdots$ stacking sequence with 10% faulting; (b) $c=14.612$ Å and a mixture of 40% $ABCABC\cdots$ stacking sequence with 10% faulting and 60% $AaAa\cdots$ stacking sequence (where a is the mirror of A), and (c) $c=14.612$ Å and an $AaAa\cdots$ stacking sequence. The (003) reflections have been truncated for clarity. For each simulation, the associated stacking sequence is illustrated at the right of the pattern.

In order to determine the changes observed in the measured XRD patterns as a function of temperature, simulation XRD patterns, shown in Fig. 8, were generated using DIFFaX (Ref. 29) (a computer program for calculating powder-diffraction intensities associated with crystals having coherent, planar defects). These three simulation patterns are to be compared with the measured patterns for the temperatures 25, 75, and 150 °C and were obtained using the atomic positions based on the crystal structures of sjögrenite and pyroaurite.[28] The pattern associated with 25 °C was generated using cell parameters $a=3.073$ Å and $c=22.713$ Å and an $ABCABC\cdots$ stacking sequence with 10% faulting. The pattern associated with 75 °C was generated using cell parameters $a=3.073$ Å and $c=14.612$ Å and a mixture of 40% $ABCABC\cdots$ stacking sequence with 10% faulting and 60% $AaAa\cdots$ stacking sequence (where a is the mirror image of A). The pattern associated with 150 °C was generated using cell parameters $a=3.073$ Å and $c=14.612$ Å and an $AaAa\cdots$ stacking sequence. A sketch of the overall stacking sequence for each simulation is shown to the right in Fig 8. It is clear from these simulations that the relative intensity changes as a function of temperature seen in the measured XRD patterns are associated with a change in the stacking sequence of the host layers.

At 25 °C the (Cl)(ZnAl):LDH material exhibits an $ABCABC\cdots$ stacking sequence which is referred to as a $3R$ polytype[16] (i.e., rhombohedral with three layers in the unit cell) and thus corresponds to the rhombohedral space group $R\bar{3}m$. At 150 °C the (Cl)(ZnAl):LDH material exhibits an $AaAa\cdots$ stacking sequence which is referred to as a $2H$ polytype[16] (i.e., hexagonal with two layers in the unit cell) and thus corresponds to the hexagonal space group $P6_3/mmc$. In the early literature,[27,28] materials which are

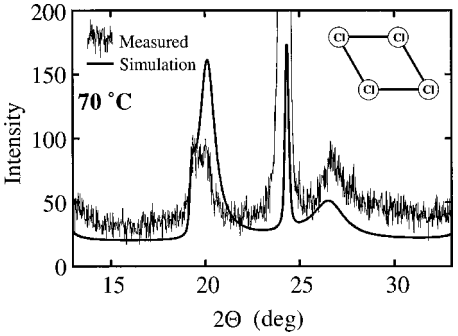

FIG. 9. A highlight of the measured Cu$K\alpha$ x-ray powder-diffraction pattern of (Cl)(ZnAl):LDH at a sample temperature of 70 °C compared to a simulated powder pattern for a $(\sqrt{3}\times\sqrt{3})R30°$ Cl ion superlattice having a stacking vector (0,0,1), (1/3,2/3,1), or (2/3,1/3,1) chosen at random. The unit cell of the Cl ions is shown in the inset.

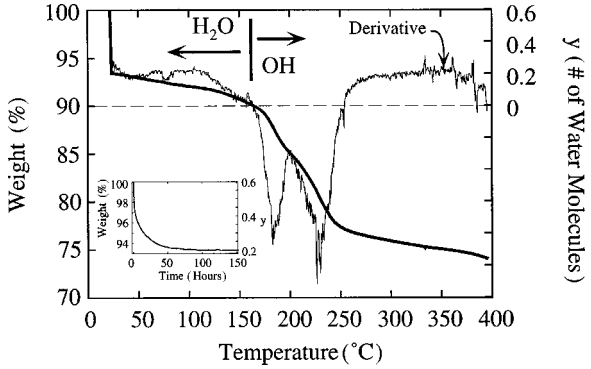

FIG. 10. The TGA weight loss (in weight %) and the derivative curve as a function of sample temperature in an N_2 purge for (Cl)(ZnAl):LDH. The number of water molecules (y) as calculated from the chemical formula is noted on the right ordinate. The dotted line refers to the fully dehydrated material ($y=0$). The sample weight was allowed to reach equilibrium in the N_2 purge at room temperature prior to starting the temperature ramp (note the drop in weight % at ~25 °C). Inset: the TGA weight loss as a function of time in the N_2 purge at room temperature as the sample weight was allowed to reach equilibrium.

now known to differ only in their stacking sequence were given different names—for example, pyroaurite/sjögrenite, hydrotalcite/manasseite, and stichtite/barbertonite.[16] Each of these pairs of LDH compounds have the same chemical formula but exhibit a $3R$-polytype/$2H$-polytype stacking sequence, respectively.

C. Cl ion superlattice

The XRD patterns shown in Fig. 6 also reveal broad, low intensity reflections in the angular range $15\leqslant 2\theta\leqslant 30°$ which are not visible in the XRD pattern measured with the sample temperature at 25 °C but are visible in the XRD patterns measured with the sample temperature between 40 and 150 °C. Although the intensity of these reflections remains low, they do appear to become sharper at higher temperatures. The reflections, for the XRD pattern measured with the sample temperature at 70 °C, are highlighted in Fig. 9 and are compared to a simulation XRD pattern again generated using DIFFaX. The simulation is based on a $(\sqrt{3}\times\sqrt{3})R30°$ Cl ion superlattice where a stacking vector (0,0,1), $(\frac{1}{3},\frac{2}{3},1)$, or $(\frac{2}{3},\frac{1}{3},1)$ is assigned at random to adjacent layers. The unit cell is shown in the inset of Fig. 9 for this structure. Given that the (Cl)(ZnAl):LDH material at higher temperatures exhibits a $2H$ polytype, the only available sites which allow a commensurate guest layer of Cl ions to stack with these vectors are the trigonal pockets directly over the metal host layer ions.

D. Hydration dynamics

Three distinct types of water molecules have been associated with LDH materials—extrinsic surface water molecules, pore water molecules and intrinsic water molecules.[30,7] Extrinsic surface water molecules are adsorbed at the outer surfaces of LDH microcrystallites. Pore water molecules fill the pore space between small diameter microcrystallite particles in a power sample. Intrinsic water molecules are intercalated into the gallery to become part of the guest layer. For the materials utilized in this study, the number of water molecules determined from chemical analysis and initial TGA measurements is equal to the number of guest layer sites that are not occupied by the charge compensation anions. Additionally, as observed in the SEM micrograph shown in Fig. 7, these materials are comprised of crystallites as large as 10 μm in diameter. Such large crystallites reduce the space available to pore water molecules as compared to materials comprised of smaller diameter microcrystallite particles. Thus we conclude that all of the extrinsic surface and pore water molecules have been removed from the materials utilized in this study. Therefore all the weight loss associated with a change in humidity will be attributed to the removal of guest layer water molecules. The weight loss associated with an increase in temperature, below some value at which the host layer begins to dehydroxylate, will also be attributed to the removal of guest layer water molecules.

Figure 10 shows TGA data from the (Cl)(ZnAl):LDH material where the initial weight loss in the N_2 purge at room temperature is shown in the inset and the remaining weight loss up to 400 °C is shown in the main panel. With all of the weight loss attributable to the removal of guest layer water molecules, the amount of guest layer water molecules (y) can be calculated as a function of temperature and is so noted on the right-hand axis of each plot. Because $y=0$ at 165 °C, the weight loss below 165 °C is associated with a dehydration of the material and above 165 °C, with a dehydroxylation of the material. This interpretation is corroborated by the XRD patterns in Fig. 6 where, despite the change in stacking sequence, it is observed that below 165 °C all of the Bragg reflections are narrow and well formed. The sharp (00L) reflections indicate regularly spaced layers of uniform thickness and the unchanged (100) and (110) reflections indicate a host layer which is unaltered. At 150 °C, the (00L) reflections begin to exhibit broad features indicating that some of the host layers are no longer either regularly spaced or of uniform thickness. By 175 °C the in-plane reflections have almost vanished indicating a severe degradation of the crystallinity of the material which would be expected as hydroxyl ions are removed from the host layer.

Similar XRD and TGA data have been measured for all the samples utilized in this study. For the CO_3 end-member

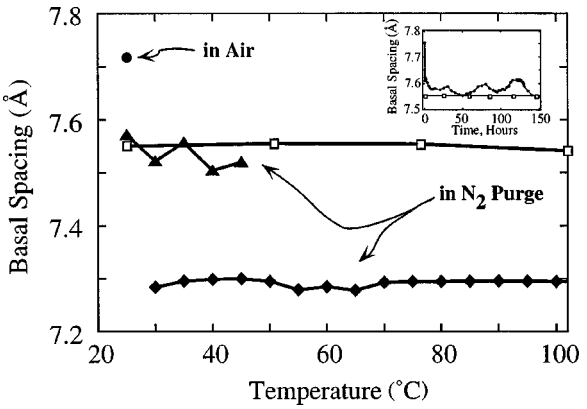

FIG. 11. The basal spacing of (Cl)(ZnAl):LDH (filled points) and (CO_3)(ZnAl):LDH (open points) as a function of temperature in an N_2 purge. Also shown is the basal spacing of both materials at room temperature in air. Note that the room-temperature basal spacing of (CO_3)(ZnAl):LDH is the same in the N_2 purge and air. Inset: the basal spacing of (Cl)(ZnAl):LDH (filled points) and (CO_3)(ZnAl):LDH (open points) as a function of time in an N_2 purge.

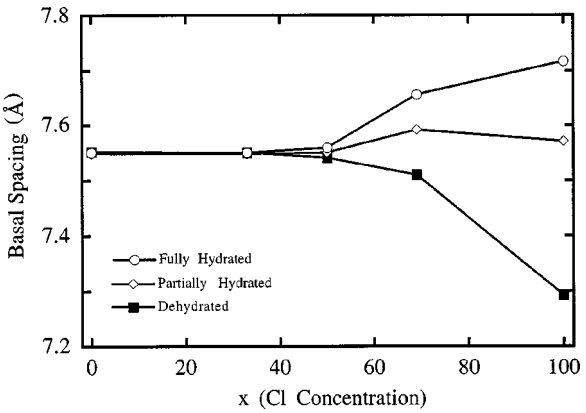

FIG. 12. The basal spacing of (CO_3/Cl)(ZnAl):LDH as a function of Cl ion concentration (x) for fully hydrated samples (open circles), partially hydrated samples (open diamonds), and dehydrated samples (filled squares).

material, it has been determined that the onset of dehydroxylation occurs at a temperature of 120 °C. By 150 °C the XRD pattern for this material also exhibits a sharp degradation of the in-plane reflections. In this paper we will focus our attention on temperature regions below which any appreciable dehydroxylation occurs and thus address only the issues associated with hydration dynamics.

The basal spacing as a function of time in the N_2 purge at room temperature (inset) and as a function of temperature (main panel) for both the CO_3 and Cl end-member materials are shown in Fig. 11. The basal spacing of the CO_3 end-member material (open squares) is about 7.55 Å and essentially independent of temperature. The basal spacing of the Cl end-member material (filled circles), however, changes dramatically with temperature. Not only does the basal spacing decrease when going from an air to a nitrogen environment, but it also exhibits a two-phase coexistence region in the temperature range $30 \leqslant T \leqslant 45$ °C. As seen in the inset in Fig. 11, the basal spacing of the Cl end-member material is initially 7.735 Å in air at room temperature and both decreases to and fluctuates around 7.6 Å while in an N_2 purge at room temperature. Based on TGA data as a function of time in the N_2 purge at room temperature (see the inset in Fig. 10) this basal spacing fluctuation is associated with a partially dehydrated sample and will be described in more detail below.

As the material is heated, the presence of the two-phase coexistence region indicates that some regions of the sample remain partially hydrated while other regions become fully dehydrated. By 50 °C, the basal spacing appears to be fully collapsed even though the TGA measurements indicate that the material is not fully dehydrated until about 150 °C. Because XRD measures the average state of a sample, this indicates that, even though some small regions of the material may not be fully dehydrated, on average, most regions of the material are dehydrated and thus the average basal spacing appears to be fully collapsed.

Before discussing the active nature of the guest layer water molecules in the Cl end-member material and presenting a model which accounts for the observed properties, we first address the basal spacing response to changes in the relative concentration of guest layer anions. Figure 12 shows the basal spacing vs Cl concentration for the series of LDH materials under three different conditions. The first curve (open circles) is for samples in air at room temperature, the second curve (open diamonds) is for the same samples at room temperature in an N_2 purge, and the third curve (filled squares) is for the same samples in an N_2 purge at 70 °C. These three curves correspond to the series of materials in a fully hydrated state, partially hydrated state, and dehydrated state. As will be discussed in more detail below, typically the basal spacing of a layered solid increases in a superlinear fashion as the concentration of the larger intercalated ion is increased.[31] For these materials, no such expansion is observed. Not only does the basal spacing of the hydrated materials increase in a sublinear fashion, but the partially hydrated materials show almost no expansion at all and the basal spacing for the dehydrated materials actually decreases as the concentration of the larger Cl anion increases.

In order to develop a model to describe the unique basal spacing dynamics of these materials, let us look in detail at the size of and interactions between species which inhabit the guest layer. Because the Cl ion is spherical, its height and in-plane diameter are both 3.62 Å .[32] the CO_3 ion, however, is asymmetric in shape with a height of 3.09 Å (Ref. 9) and an in-plane diameter of about 6 Å as determined from close-packing of hard spheres. For the CO_3 ion, its height together with the host layer thickness $t = 4.46$ Å (Ref. 11) would produce a basal spacing of 7.55 Å , provided that the CO_3 ion is not nested within the trigonal pockets of the host layer and that its threefold axis is perpendicular to the host layer. This is precisely the basal spacing measured for the CO_3 end-member material in air at room temperature. Since the data in Figs. 11 and 12 indicate that the basal spacing of the (CO_3/Cl)(ZnAl):LDH materials with $x < 0.5$ is independent of humidity, temperature, and ionic concentration, we conclude that the CO_3 ions are always oriented with their threefold axis perpendicular to the host layer. The basal spacing dynamics must therefore be related to the Cl ions.

The height difference between the Cl and CO_3 ions is $\Delta h = 0.53$ Å , yet the largest basal spacing differences (see

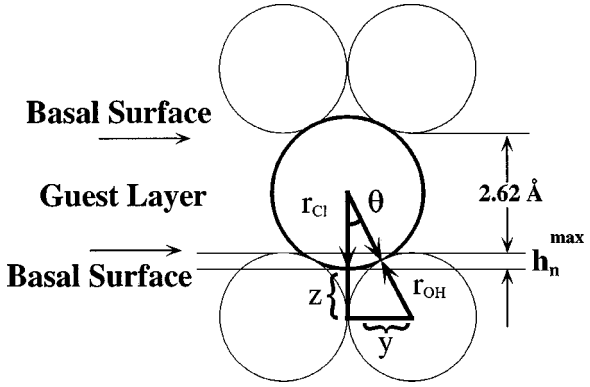

FIG. 13. A diagram of the nesting of a guest layer Cl ion (circle with thick line) into trigonal pockets of the basal spacing generated by closed-packed hydroxyl ions (circles with thin line). The maximal nesting height is shown as $h_n^{\max}$.

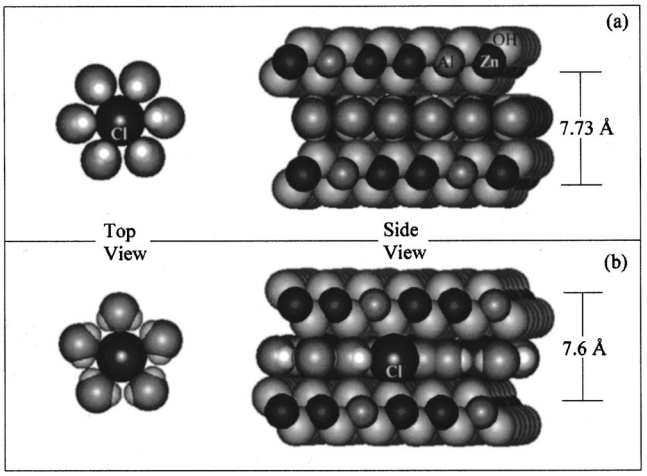

FIG. 14. A schematic diagram of the proposed (a) six-member and (b) five-member hydration rings surrounding the Cl ion in the guest layer. Both the top view (left) and side view (right) are shown (Ref. 15).

Fig. 12) is only 0.25 Å between the dehydrated end-member materials where the large Cl ion is associated with the smaller basal spacing. This implies that the Cl ion is nested into the trigonal pockets of the host layer. The degree to which the Cl ion is nested into one trigonal pocket can be expressed by the equation

$$h_n^{\text{meas}} = r_{\text{Cl}} - \tfrac{1}{2}(d_{\text{Cl}} - t), \tag{1}$$

where $r_{\text{Cl}} = 1.81$ Å is the radius of a Cl ion, $d_{\text{Cl}} = 7.293$ Å is the basal spacing of the dehydrated (Cl)(ZnAl):LDH material, and $t = 4.46$ Å is the host layer thickness, thus $h_n^{\text{meas}} = 0.39$ Å. If we employ a hard-sphere model, as shown in Fig. 13, where the basal surface is comprised of close-packed hydroxyl ions of radius $r_{\text{OH}} = a/2 = 1.537$ Å then the maximal nesting of a Cl ion can be expressed as

$$h_n^{\max} = [r_{\text{Cl}} + r_{\text{OH}}](1 - \cos\Theta), \tag{2}$$

where

$$\Theta = \sin^{-1}\left[\frac{2}{\left\{\sqrt{3}\left(1 + \frac{r_{\text{Cl}}}{r_{\text{OH}}}\right)\right\}}\right]. \tag{3}$$

The maximal nesting value for the Cl ion into a trigonal pocket is thus calculated to be $h_n^{\max} = 0.5$ Å . This indicates that the Cl ions are approximately 78% nested for the dehydrated (Cl)(ZnAl):LDH material. This degree of nesting is sensible given that h_n^{meas} represents an average value over all Cl sites and that the weak nature of the Cl ion superlattice reflections implies an absence of long-range order (i.e., the Cl ions are not all sitting precisely in equivalent sites). The Cl ion can now be viewed as possessing an effective height $h_{\text{Cl}}^{\text{eff}} = 2.84$ Å thus making it the smaller of the two guest layer anions.

For the partially hydrated materials, we have seen that the basal spacing is independent of x. The Cl ion must still be, at least partially, nested, otherwise the larger height of the full ion would manifest itself as an increase in the basal spacing. Because Cl is strongly electronegative, the water molecules that are now present in the guest layer will tend to solvate the Cl ions. A hard-sphere model allows up to five water molecules with the plane of the molecule parallel to the basal surface to form a planar hydration ring around a nested Cl ion as shown in the bottom panel of Fig. 14.[11] So long as the tilt angle (i.e., the angle of rotation around the C_{2v} axis of a water molecule referenced to the basal surface) is small, the resulting solvated ion will have an in-plane radius of about 4.6 Å and a height defined by the oxygen atom. Since the height of the CO_3 ion is also defined by the oxygen atom, it is reasonable to expect the basal spacing of a partially hydrated (CO_3/Cl)(ZnAl):LDH material to be independent of x. As long as some water molecules are in the guest layer, it is also reasonable to expect the basal spacing to be independent of y up to the point where Cl ion hydration ring consists of a maximum of five water molecules. The concept of a Cl ion hydration ring can be extended for the fully hydrated materials where the number of solvating water molecules exceeds five. For large tilt angles, up to six water molecules can form a hydration ring around a nested Cl ion as shown in the top panel of Fig. 14.[11] The height of the solvated Cl ion is no longer defined by the oxygen atom but rather by the size of the tilted water molecule. Thus the basal spacing resulting from a solvated Cl ion containing six water molecules is larger than that resulting from a solvated Cl ion containing five water molecules.

The number of water molecules available to solvate a given Cl ion within the (Cl)(ZnAl):LDH material can be simulated by an ordered arrangement of Cl ions onto a $(\sqrt{3} \times \sqrt{3})R30°$ commensurate structure. The remaining sites are then occupied by water molecules, thus creating a fully hydrated model of the $x = 1$, $y = 0.6$ material. This model provides the correct number of charge compensating anions and water molecules based on chemical analysis and is consistent with the superlattice structure observed for the dehydrated (Cl)(ZnAl):LDH material. In this model, the Cl ions have six nearest-neighbor water molecules. Dehydration can be simulated by removing some of the water molecules and a change in anionic concentration can be simulated by replacing two Cl ions and one water molecule with one CO_3 ion. At $x = 1$, dehydrating to the point where most Cl ions have five nearest-neighbor water molecules corresponds to $y = 0.5$. Based on this model, the basal spacing is predicted to sharply

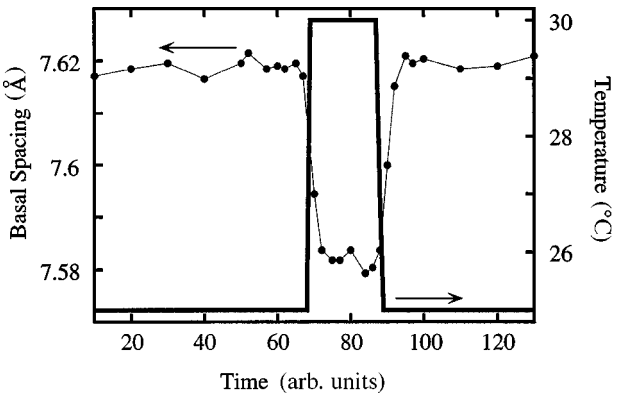

FIG. 15. The basal spacing and sample temperature as a function of time for (Cl)(ZnAl):LDH in an N_2 purge.

decrease at $y=0.5$ for the Cl end-member material. The inset in Fig. 11 indicates that approximately 20 min after the (Cl)(ZnAl):LDH sample enters an N_2 purge, the number of guest layer water molecules is reduced to $y=0.5$. It is precisely at this point where the basal spacing, shown in the inset in Fig. 11, sharply decreases for the (Cl)(ZnAl):LDH material.

For the model material, in a fully hydrated state at $x=0.5$, the number of Cl ions is double the number of CO_3 ions and the remaining sites in the guest layer are occupied by water molecules. This results in each Cl ion having five nearest-neighbor water molecules. Based on this model, the basal spacing should remain unchanged for $x<0.5$ and should increase for $x>0.5$ for the fully hydrated materials. This prediction describes precisely what is seen in Fig. 12 for the fully hydrated materials. At $x=0$, there are no Cl ions present in the model material, thus the water molecules are viewed as passive members of the guest layer and the basal spacing is predicted to be independent of the number of water molecules in the guest layer. Again this is consistent with what has been observed in Fig. 11 for the basal spacing of the CO_3 end-member material.

The room-temperature, basal spacing fluctuations observed in the partially hydrated, Cl end-member material (see the inset in Fig. 11) can now be understood in terms of the hydration dynamics. When a Cl end-member sample enters the N_2 purge at room temperature, the basal spacing decreases from 7.735 to 7.6 Å within the first 20 min. At this time, each Cl ion has five nearest-neighbor water molecules as has been described above. TGA data shown in the inset in Fig. 10 indicate that the sample continues to dehydrate to the point where each Cl ion has two nearest-neighbor water molecules. Since the number of water molecules steadily decreases with elapsed time in the N_2 purge, the fluctuations do not appear to be directly related to the water content in the guest layer. Figure 15 shows the basal spacing response to small ($\sim 5\,^{\circ}C$) changes in sample temperature. Here the temperature of the sample was specifically controlled by the sample heater and temperature controller as opposed to floating at room temperature. It is clear from this figure that the basal spacing fluctuations seen in the inset of Fig. 11 are related to room-temperature fluctuation. As discussed above, less than five water molecules can form a planar hydration ring around a Cl ion in the guest layer. These molecules, however, are not constrained to lie in the plane of the guest layer but can rotate about their C_{2v} axis in a rotational potential well defined by the bounding host layers. This rotation is a thermally activated process and the larger the rotation angle, the more the water molecules cause the basal spacing to increase. As the room temperature fluctuates, so does the average rotation angle of the water molecules around their C_{2v} axis and therefore so does the average basal spacing.

E. Layer rigidity

The layer rigidity of graphite, layered dichalcogenides, and alumino-silicate clays has been studied using the discrete finite layer rigidity (FLR) model.[33–35] This model is constructed on the basis of a layered solid having guest layer ions of height h_A intercalated between host layers of thickness t such that the basal spacing is defined to be $d=t+h_A$. If a smaller A ion is replaced by a larger B ion then the host layer will pucker to form a catchment area around the larger ion. This catchment area contains an average of p lattice sites and the normalized basal spacing, which is by definition

$$d_n(x)=\frac{d(x)-d(0)}{d(1)-d(0)}, \tag{4}$$

can be written as

$$d_n(x)=1-(1-x)^p, \tag{5}$$

where p is referred to as the interlayer rigidity parameter.[10] This model assumes that (i) the host layer composition is independent of the guest layer composition, (ii) the host layer thickness remains constant and is thus independent of the degree of puckering imposed by the larger guest layer ion, and (iii) the A and B ions are rigid and of fixed height.

As noted in the Introduction, the layer rigidity of LDH's was initially studied using (CO_3)(NiAl):LDH's which is a series of variable-host layer materials.[9] These materials, however, violate the first assumption of the FLR model because the host layer composition is a function of the guest layer composition. While the basal spacing can indeed be modeled by an extended version of the FLR model,[9] the results cannot be accurately compared with that of fixed-host layered solids. It is thus desirable to study a series of fixed-host layer LDH materials in order to obtain a more direct and accurate measure of the interlayer rigidity parameter which can be compared to previous layer rigidity studies of other layered solids. The (CO_3/Cl)(ZnAl):LDH's are just such a series of fixed-host layer materials. The composition-dependence of their basal spacing has already been presented in Fig. 12 for fully hydrated, partially hydrated and dehydrated materials. The hydration dynamics associated with these three curves have also been discussed in detail. We now discuss these curves in terms of the discrete FLR model.

Even though the basal spacing for the fully hydrated material increases as a function of the concentration of the larger guest layer ion, it does not fit the standard superlinear form of the FLR model. This results because the effective height of the solvated Cl ion is a function of the concentration of the ion itself. This is a violation of the third assumption of the FLR model which states that the height of the ion

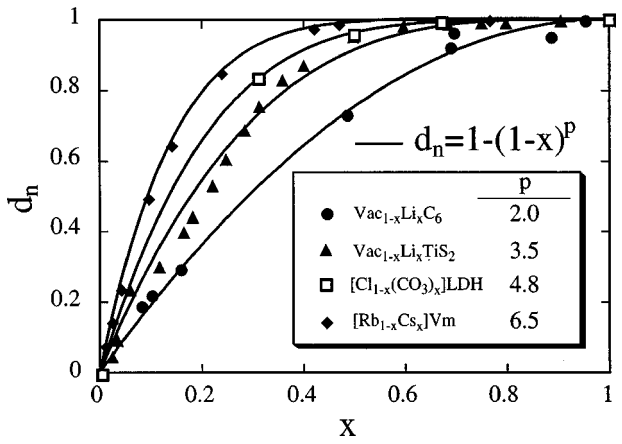

FIG. 16. The normalized basal spacing vs concentration (x) for Li_xC_6 (circles), Li_xTiS_2 (triangles), $Cl_{1-x}(CO_3)_x$(ZnAl):LDH (squares), and $Rb_{1-x}Cs_x$ vermiculite (diamonds). The error bars are smaller than the data points for each material. The solid lines represent a fit of the FLR model [Eq. (5)] to each data set. The interlayer rigidity parameter (p) determined from each fit is shown in the legend.

is assumed to be fixed. For the partially hydrated materials, the basal spacing is independent of the relative concentration of guest layer ions. This results because the heights of both the CO_3 ion and the solvated, nested Cl ion are defined by the size of an oxygen atom. That is to say, $h_A = h_B$ in the FLR model which violates the definition of h_A and h_B as the heights of different size ions. In both of these cases, the presence of water molecules in the guest layer violates key assumptions of the FLR model.

In order to successfully apply the FLR model it is necessary to remove the guest layer water molecules as has been done for the dehydrated materials. The curve associated with the dehydrated materials has the necessary superlinear form; however, the basal spacing is larger for the smaller ion. As discussed above, this retrograde response results from the fact that the nested Cl ion has an effective height that is actually less than the height of the CO_3 ion. This can be reconciled by letting h_A be the effective height of the nested Cl ion and h_B be the height of the CO_3 ion which is equivalent to plotting the basal spacing as a function of the CO_3 ion concentration rather than the Cl ion concentration. The data for the dehydrated (CO_3/Cl)(ZnAl):LDH materials are so plotted in Fig. 16 along with the normalized basal spacings for several other layered solids which are shown for comparison and which have been previously analyzed[12–14] using the FLR model. The discrete FLR model has been fit to all the curves in this plot (lines) with the results included in the figure where $p = 4.84 \pm 0.06$ for the LDH. Here the FLR model is successfully applied to the fixed-host layer LDH materials and the results compare directly with those of other layered solids. LDH materials are seen to be stiffer than class-II layered solids such as the dichalcogenides but not as stiff as class-III layered solids such as alumino-silicate clays. These results also validate the previous results from the variable-host layer materials where the interlayer rigidity parameter was determined to be $p \sim 5$ as compared to $p = 4.84 \pm 0.06$ for the fixed-host layer materials.

IV. SUMMARY AND CONCLUSIONS

The fixed-host layer LDH materials, (CO_3/Cl)(ZnAl):LDH, exhibit unique basal spacing dynamics due to the interplay between strongly electronegative Cl anions and guest layer water molecules. The height of the bare Cl ion is larger than that of the CO_3 ion, however, the in-plane diameter of the CO_3 ion is larger than that of the Cl ion. Therefore the CO_3 ion is prevented from nesting while the Cl ion can nest into the trigonal pockets of the bounding host layers. For the dehydrated materials, the nested height of the Cl ion is smaller than the height of the CO_3 ion resulting in a retrograde response where the basal spacing due to the larger, yet nested, Cl ion is smaller that the basal spacing due to the smaller CO_3 ion. For the partially hydrated material, up to five guest layer water molecules, with the plane of the molecule parallel to the host layer, can form a hydration ring around the Cl ion. Since the height of a CO_3 ion and a water molecule having a small tilt angle are defined by the size of the oxygen atom, the basal spacing is independent of ionic concentration. For fully hydrated materials above $x = 0.5$, each Cl ion has, on average, more than five nearest-neighbor water molecules. In order to form a six-member hydration ring around the Cl ion, the water molecules must tilt around their C_{2v} axis. This large tilt angle causes a water molecule to become an active member of the guest layer because it now has a height larger than both the nested Cl ion and the CO_3 ion. This active nature of the water molecules causes the basal spacing to be not only a function of ionic concentration (x) but also a function of hydration (y).

For the (CO_3/Cl)(ZnAl):LDH materials, the Cl end-member ($x = 1$) is the only material to exhibit a change in stacking sequence upon dehydration. In the fully hydrated form, the material exhibits a $3R$ stacking sequence. In the dehydrated form, the material exhibits a $2H$ stacking sequence. Also in the $x = 1$ dehydrated material, the Cl ions form a $(\sqrt{3} \times \sqrt{3})R30°$ in-plane superlattice.

Because the height of the solvated, nested Cl ion is equal to the height of the CO_3 in the partially hydrated material and is a function of hydration in the fully hydrated material, the discrete finite layer rigidity model can be used to study the layer rigidity of only the dehydrated materials. With the nested Cl ion as the smaller member of the guest layer, a fit of the FLR model to the normalized basal spacing vs CO_3 ionic concentration produces an interlayer rigidity parameter $p = 4.84 \pm 0.06$. This value for the fixed-host LDH's validates previous work on variable-host layer LDH materials which produced an interlayer rigidity parameter $p \sim 5$. When compared to previous work on other layer solids, the LDH's are found to be stiffer than dichalcogenides but not as stiff as alumino-silicate clays.

ACKNOWLEDGMENTS

We wish to thank M. M. J. Treacy for useful discussions and assistance with regard to the DIFFaX simulation program. Two of us (U.C. and M.N.) thank MURST, Italy for financial support.

[1] F. Cavani, F. Trifirò, and A. Vaccari, Catal. Today **11**, 173 (1991).
[2] F. Trifirò and A. Vaccari, in *Comprehensive Supramolecular Chemistry*, edited by G. Alberti and T. Bein (Pergamon, New York, Elsevier Science, New York, Oxford University, New York, 1996), Vol. 7, Chap. 8.
[3] G. A. O'Neill, J. W. Novak, and E. S. Martin, U.S. Patent No. 4,935,146 (1990).
[4] H. Tagaya, A. Ogata, T. Kuwahara, S. Ogata, M. Karasu, J. Kadokawa, and J. Chiba, Microporous Mater. **7**, 151 (1996); E. P. Giannelis, D. G. Nocera, and T. J. Pinnavaia, Inorg. Chem. **26**, 203 (1987).
[5] J. O. Besenhard, in *Progress in Intercalation Research*, edited by W. Muller-Warmuth and R. Schollhorn (Kluwer, Boston, 1994), p. 457.
[6] S. A. Solin, in *Intercalation in Layered Materials*, edited by M. S. Dresselhaus (Plenum, New York, 1986), p. 291.
[7] A. de Roy, C. Forano, K. E. Malki, and J. P. Besse, *Expanded Clays and Other Miscoporous Solids* (Van Nostrand Reinhold, New York, 1992), Vol. 2, p. 108.
[8] N. Wada, D. Hines, and S. P. Ahrenkiel, Phys. Rev. B **41**, 12 895 (1990).
[9] S. A. Solin, D. R. Hines, S. K. Yun, T. J. Pinnavaia, and M. F. Thorpe, J. Non-Cryst. Solids **182**, 212 (1995).
[10] M. F. Thorpe, Phys. Rev. B **39**, 10 370 (1989).
[11] D. R. Hines, S. A. Solin, U. Costantino, and M. Nocchetti, Solid State Commun. **108**, 971 (1998).
[12] *Graphite Intercalation Compounds II: Structure and Dynamics*, edited by H. Zabel and S. A. Solin (Springer-Verlag, Berlin, 1992), p. 433.
[13] *Crystal Chemistry and Properties of Materials with Quasi One-Dimensional Structure*, edited by J. Rouxel (Reidel, Boston, 1986).
[14] T. J. Pinnavaia, Science **990**, 365 (1983).
[15] D. R. Hines, S. A. Solin, U. Costantino, and M. Nocchetti (unpublished).
[16] H. F. W. Taylor, Miner. Mag. **39**, 377 (1973).
[17] U. Costantino, F. Marmottini, M. Nocchetti, and R. Vivani, Eur. J. Inorg. Chem. **1998**, 1439.
[18] F. Hellferich, *Ion Exchange* (McGraw-Hill, New York, 1962), p. 151.
[19] A. I. Vogel, *Vogel's Textbook of Quantitative Chemical Analysis*, 5th ed., revised (Longmann Scientific & Technical, Harlow, UK, 1989).
[20] B. R. York, S. A. Solin, N. Wada, R. H. Raythatha, I. D. Johnson, and T. J. Pinnavaia, Solid State Commun. **54**, 475 (1985).
[21] W. T. Riechle, Solid State Ionics **22**, 135 (1986).
[22] D. L. Bish and G. W. Brindley, Am. Mineral. **62**, 458 (1977).
[23] See Ref. 18, Chap. 4.
[24] R. M. Barrer and J. D. Falconer, Proc. R. Soc. London, Ser. A **236**, 227 (1956).
[25] G. Alberti, Acc. Chem. Res. **11**, 163 (1978).
[26] J. Inczedy, *Analytical Application of Ion Exchangers* (Pergamon, New York, Oxford University, New York, 1966), p. 44.
[27] R. Allmann and H. P. Jepsen, Neues Jahrb. Mineral., Monatsh. **1969**, 544.
[28] L. Ingram and H. F. W. Taylor, Miner. Mag. **36**, 465 (1967).
[29] M. M. J. Treacy, J. M. Newsam, and M. W. Deem, Proc. R. Soc. London, Ser. A **433**, 499 (1991).
[30] S. K. Yun and T. J. Pinnavaia, Chem. Mater. **7**, 348 (1995).
[31] S. Lee, H. Miyazaki, S. D. Mahanti, and S. A. Solin, Phys. Rev. Lett. **62**, 3066 (1989).
[32] *Handbook of Chemistry and Physics*, 60th ed., edited by R. C. Weast (CRC, Cleveland, OH, 1980).
[33] J. E. Fisher and H. J. Kim, Phys. Rev. B **35**, 3295 (1987).
[34] J. R. Dahn, D. C. Dahn, and R. R. Haering, Solid State Commun. **42**, 179 (1982).
[35] H. Kim, W. Jin, S. Lee, P. Zhou, T. J. Pinnavaia, S. D. Mahanti, and S. A. Solin, Phys. Rev. Lett. **60**, 2168 (1988).